PROCESS-INDUCED DISTORTION PREDICTION FOR LAMINATED COMPOSITES

Shuang Yan, Mikhail Matveev and Nicholas Warrior

Composites Research Group, Faculty of Engineering, University of Nottingham, Nottingham, UK

Keywords: Residual stress, Process-induced distortions, Laminated composites, Finite element analysis

ABSTRACT

Residual stresses developed in laminates during autoclave processing often leads to distortion such as spring-in and warpage. In this study, the effects of the thickness, corner radius and flange length were investigated experimentally and numerically. A coupled thermal-chemical-mechanical modelling approach was developed to predict spring-in angle of L-shaped laminates. A semi-empirical approach was proposed to estimate the spring-in angle induced by tool-part interaction, reducing computational cost compared with direct modelling of the tool. This paper demonstrates that geometric features can have a significant impact on spring-in and warpage.

1 INTRODUCTION

Though properties of composite laminates can be tailored by designing its layup, one should pay attention to the process-induced distortions during the manufacturing process. Finding the contributing factors to the process-induced distortions or residual stresses has long been the key motivation in the aerospace and other industries.

In the manufacturing of a curved composites structure, the enclosed angle tends to be reduced after demoulding. This phenomenon is referred as 'spring-in' [1]. By nature, fibre reinforced laminates exhibit anisotropic behaviour due to the significant differences between the coefficient of thermal expansion (CTE) in fibre direction and that in off-axis directions. During the cooling-down phase, thermal contraction occurs, contributing to the reduction in enclosed angle. In a similar manner, prior to cooling down, resin shrinkage takes place, since resin is more dominant in the through-thickness direction compared with that in fibre direction, more shrinkage occurs in resin-rich areas. Figure 1 shows a comparison of isotropic and anisotropic shrinkage, as an illustration of spring-in mechanism.

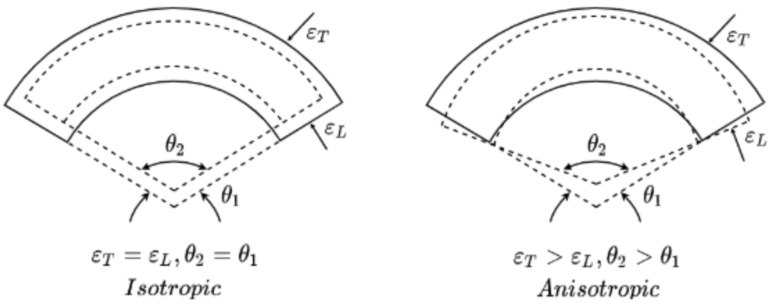

Figure 1 Mechanism of spring-in phenomenon

Another form of distortion is referred as warpage, commonly observed in flat components when demoulded. As per industry standard, prepregs are symmetrically laminated to achieve quasi-static equilibrium, in rare case of asymmetrical lamination, warpage would be expected. Other case of inducing warpage is contributed from the CTE difference of the laminates and that of the mould. Typically, an aluminium or steel tool would have larger CTE compared with laminated composites, causing friction at the interface. In real life scenario, distortions are often seen in a combined form of spring-in and warpage.

2 EXPERIMENTAL INVESTIGATIONS ON SPRING-IN PHENOMENON

2.1 Experimental procedures

Hexcel IM7/8552 unidirectional prepregs were used to conduct an experimental investigation of spring-in phenomenon exhibited in L-shaped laminates. The IM7 carbon fibre is a continuous, high performance, intermediate modulus, PAN-based fibre in 12K filament count tows, while the resin 8552 is a high performance, amine cured, toughened epoxy matrix system. The average cured ply thickness for the supplied batch is 0.19 mm. Three aluminium tools were manufactured, with 0.25, 0.5 and 1 inches radius at the corner.

In this work, 30 L-shaped specimens were manufactured, shown in Figure 2. Each L-shaped specimen has a width of 60 mm and each configuration was repeated three times to mitigate scattering effects such as dimensional discrepancy from hand lay-up. The L-shaped specimens were categorised into four groups investigating the effect of varying geometrical features, including thickness, radius, flange length, and lay-up sequence, summarized in Table 1.

In addition to the L-shaped specimens, 6 flat specimens with $[0/90]_s$ lay-up were fabricated to investigate the effect of tool-part interaction. The length of the specimens measures 120 mm,180 mm and 240 mm, with a consistent width of 40 mm.

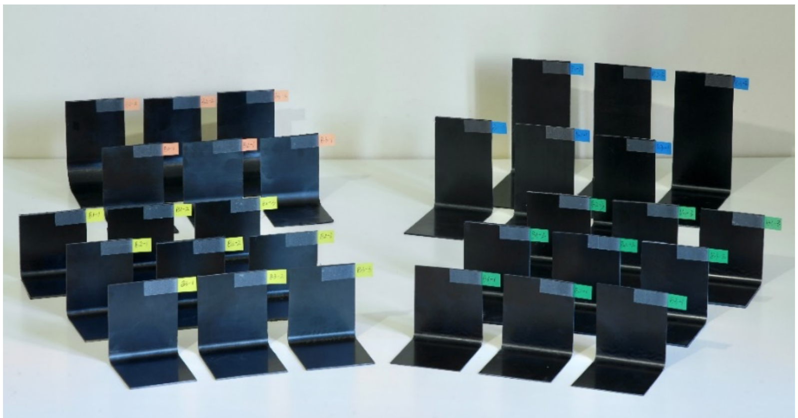

(a)

(b)

Figure 2 All the (a) L-shaped and (b) plate specimens manufactured in this work

Specimen no.	Lay-ups	radius (inch)	flange length (mm)
1	$[0/90]_s$	0.25	60
2	$[0/90]_{2s}$	0.25	60
3	$[0/90]_{3s}$	0.25	60
4	$[0/90]_s$	0.25	90
5	$[0/90]_s$	0.25	120
6	$[0/90]_s$	0.5	60
7	$[0/90]_s$	1.0	60
8	$[0/45/-45/90]_s$	0.25	60
9	$[0/90/45/-45]_s$	0.25	60
10	$[45/-45/90/0]_s$	0.25	60

Table 1 Configuration of L-shaped specimens

All the specimens were manufactured in the autoclave following manufacturing recommended cure cycle (MRCC). At the beginning of the process, 7 bar gauge autoclave pressure and full vacuum were applied. A temperature ramp of 20°C/min were applied until the ambient temperature reaches 110°C, following which, the specimens dwell at 110°C for 60 minutes. A second temperature ramp and dwell were applied afterwards, where the specimens were heated up at a rate of 2 °C/min to 180 °C and held at 180 °C for 120 minutes. The specimens were then cooled down at a rate of 3 °C/min until a target temperature of 60 °C was reached. The pressure was then vented while the vacuum was still in place.

At the end of the cure cycle, specimens were taken out of the autoclave and left to cool down to the room temperature.

2.2 Measurement of spring-in and warpage

The surface geometry of all the specimens and aluminium tools were measured using Creaform 3D HandySCAN, with a scanning precision of up to 0.2 mm. An example of scanning an L-shaped specimen depicted in Figure 3. A white powder coating spray was applied to give a matt finish on the surface of the specimens. The deflection measurement of plate specimens requires careful handling. It was found that the self-weight of the specimen could significantly affect the warpage measurement. In this study, the specimen was carefully rested on the thickness edge side with minimum support on other surfaces to eliminate self-weight effects.

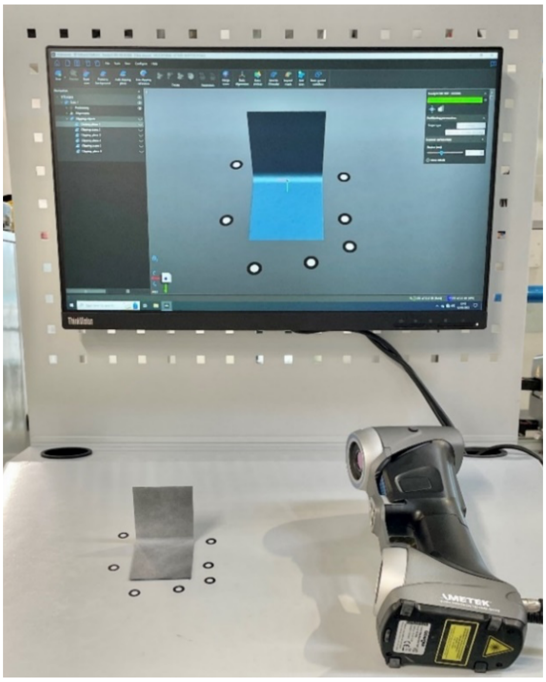

Figure 3 Measurements of L-shaped specimen using Creaform 3D HandySCAN

The deflection profile along the length of the plate specimens was obtained by processing the scanned point cloud image. Taking the specimens with 120 mm length for example, a polynomial curve was fitted to the point cloud data, as illustrated in Figure 4. The deflection is the distance to the neutral plane and the position is marked as zero at the centre of the plate. Therefore, the maximum warpage is graphically interpreted as the absolute deflection.

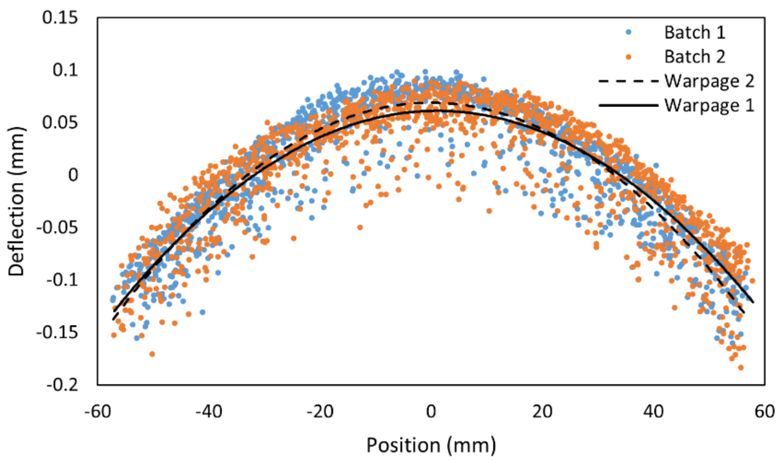

Figure 4 Warpage of the specimens with a length of 120 mm

Finding the enclosed angle of the L-shaped specimens requires post-processing of the scanned image using GOM Inspect suite. In this study, two planes were fitted to the flange parts of the scanned specimen using Gaussian best fit algorithm. The included angle was then determined by taking the angle of the normal vectors of the two fitted planes. The same method was applied to the measurement of the aluminium tools. The surfaces of the tools were hand polished, hence, subjected to small variations in the enclosed angle, therefore the scanned geometry of the tool was analysed at different locations to obtain an average measure of the enclosed angle. Measurement indicates that the maximum discrepancy in terms of tool angle is 0.03°. Having the angle profile of the L-shaped specimens and that of the aluminium tools, subtracting the angle of the measured specimen from the angle of its corresponding tool gives the spring-in angle of interest.

3 SEMI-EMPIRICAL INVESTIGATION ON TOOL-PART INTERACTION EFFECT

It was observed in this study that symmetrical and balanced laminates fabricated on a flat tool exhibit warpage after demoulding. The common explanation states such deformation is the result of the CTE mismatch between tool and part. In most cases, this mechanism is invoked when a laminate with low CTE manufactured using a tool with a significantly higher CTE, such as aluminium and steel.

At the beginning of an autoclave process, both tool and part are going through a temperature ramp subjected to autoclave pressure, ensuring a closed contact between the surface of the tool and the part. Laminates are stretched due to tool expansion under elevated temperature. Layers close to the tool surface are exposed to higher strains than those are further away, generating stress gradient through the thickness of the laminates. After the resin is cured, such stress gradient is locked in, and referred as the residual stress due to tool-part interaction. When the part is demoulded from the tool, such residual stresses are released through a concave down warpage. The magnitude of warpage deformation is associated with many factors, including tool material, tool surface finish, autoclave pressure, viscosity of the resin, the contribution of each factor varies from case to case, which are difficult to isolate.

In this study, a semi-empirical approach was proposed to substitute the tool-part friction with equivalent residual stresses causing the same warpage in the plate laminates. This friction model was later on used to predict the spring-in angle of the L-shaped laminates due to tool-part interaction only.

3.1 Analytical prediction of tool-part interaction effect

Assuming the friction is uniformly distributed across the tool-part interface, the force equilibrium at the load-bearing layer is illustrated in Figure 5, written in the form of

$$d\sigma \cdot h_s + \tau_s \cdot dx = 0 \tag{1}$$

Where h_s is the thickness of a single layer, σ is the interior shear stress component, and τ_s is the friction. The total thickness of the laminates is h, taking symmetric geometry of the 1st [0°] layer, the half-length is l and the depth is b. The distance from the 1st [0°] layer (load bearing layer) to the mid-plane is denoted as z_s and the distance from the k th layer to the mid-plane is denoted as z_k.

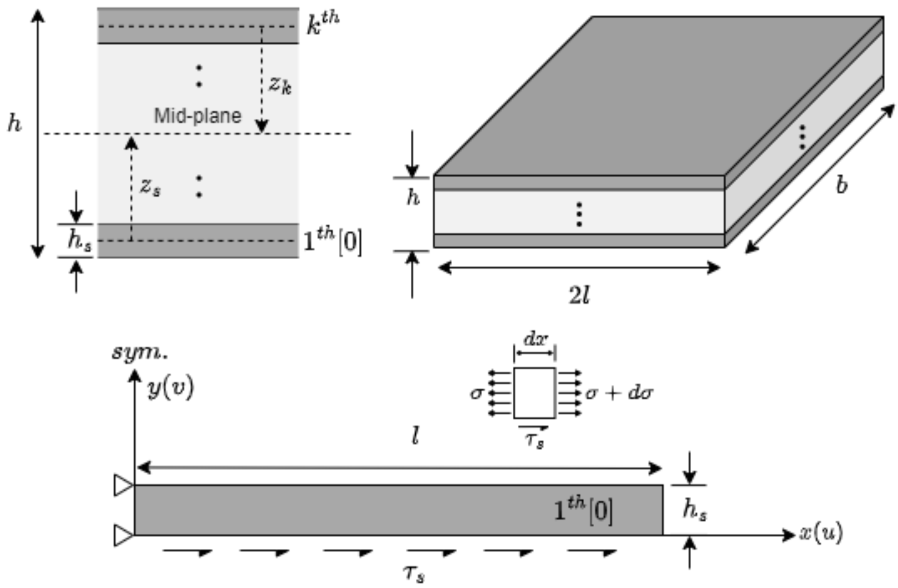

Figure 5 Force diagram of tool-part interaction

Integrating Eq.(1) and applying boundary conditions, the interface shear stress is expressed as

$$\sigma(x) = \frac{\tau_s}{h_s}(l - x) \tag{2}$$

Based on small strain theory, the curvature of a laminate is expressed as

$$\kappa = \frac{d^2 v}{dx^2} = \frac{M}{(EI)_{eff}} = \frac{\sigma \cdot h_s \cdot z_s \cdot b}{(EI)_{eff}} \tag{3}$$

Integrating Eq.(3) gives

$$v = \frac{z_s \tau_s b}{2(EI)_{eff}}\left(lx^2 - \frac{1}{3}x^3\right) \tag{4}$$

Hence, the maximum deflection can be found at $x = l$

$$v_{max} = \frac{z_s \tau_s l^3 b}{3(EI)_{eff}} \tag{5}$$

According to the classic laminate theory, the effective flexural stiffness is expressed as

$$(EI)_{eff} = \sum_{k=1}^{m} [\bar{Q}_{11}]_k \left(\frac{1}{12} {h_s}^3 + {z_k}^2 h_s\right) b \tag{6}$$

For a given length and lay-ups of a specimen, taking Eq.(6) into Eq.(5) gives the relationship between the maximum deflection and the friction at the interface.

3.2 Numerical prediction of tool-part interaction effect

The analytically derived friction τ_s from the previous section was further validated in the numerical model here. As depicted in Figure 6, a $[0°/90°]_s$ cross-ply laminate was modelled subjected to a frictional load only at the bottom of the laminate. A static analysis was performed and symmetrical boundary condition was applied. This frictional load was calibrated so that the maximum deflection fits the experimentally measured value at the middle of the laminate.

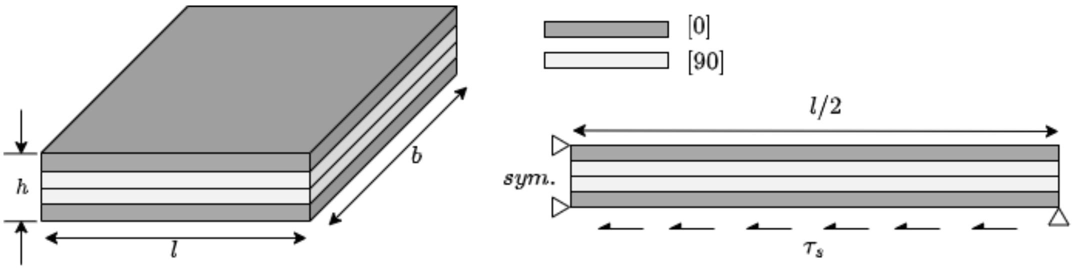

Figure 6 Model geometry and boundary conditions of the plate laminates

Length (mm)	Batch 1 (mm)	Batch 2 (mm)	Avg. Warpage (mm)	Analytical τ_s (kPa)	Numerical τ_s (kPa)
120	0.18	0.20	0.19	51.2	35.0
180	0.18	0.39	0.29	23.5	15.5
240	0.22	0.38	0.30	10.9	7.9

Table 2 Equivalent tool-part interface friction of the plate specimens

It was observed from Table 2 that the analytical method overestimates the friction at the tool-part interface compared with the numerically calibrated values. The experimental results also show that longer specimens produce higher variability in warpage. The warpage for two flat specimens with 120 mm length were relatively close, while the warpage for other two longer parts show great discrepancies. In the case of 240 mm flat specimen, warpage measurement varying from 0.2 mm to 0.4 mm could result in the friction value varying from 5.2 kPa to 10.5 kPa. Ideally, more specimens with longer length should be manufactured to provide more reliable measurements.

4 NUMERICAL INVESTIGATION ON SPRING-IN PHENOMENON

4.1 Numerical implementation in ABAQUS

In this study, the thermal-chemical analysis and mechanical analysis were sequentially coupled. In the thermal-chemical analysis, an internal heat generation term was incorporated to account for exothermic chemical reaction. Temperature and Degree-of-Cure (DoC) fields were updated at each time increment until the analysis reached the end of the MRCC. In the mechanical analysis, process-induced thermal and chemical strains were to be determined from the temperature and DoC history field. At each time increment, the effective laminate mechanical properties were updated to compute the residual stress and displacement field at the end of analysis. In this study, a Cure Hardening Instantaneous Linear Elastic (CHILE) constitutive model was employed [2]. A framework of modelling procedure with user subroutines was illustrated in Figure 7.

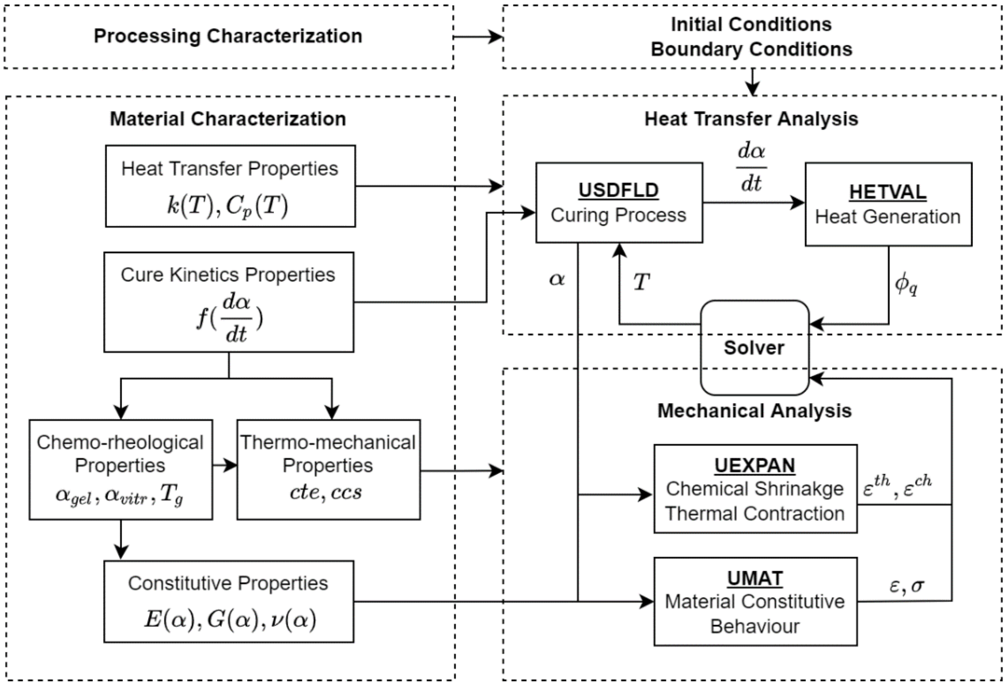

Figure 7 Modelling framework including user-subroutines

4.2 Model description

Taking advantage of symmetry, a quarter section of an L-shaped laminates was modelled, as illustrated in Figure 8. The model consists of a flange part and a 45° curved part. The inner radius of the curved part corresponds to the radius of the aluminium tool. The length of the flange was consistent to the specimen configurations. The simulation was performed in two analysis steps, namely a coupled temperature-displacement analysis, corresponding to the autoclave cure process, and a static analysis, representing the demoulding. In the autoclave cure process, the part was constrained in the normal direction at the tool-part contact surface, subjected to autoclave pressure load. The pressure and the surface support were then removed to simulate the demoulding process. One element per ply in the thickness direction was assigned in the through-thickness direction, while a sufficiently small meshing size was assigned to the arc direction. An 8-node coupled-temperature-displacement solid element C3D8T was selected. The ambient temperature was assumed to be 20°C. Surface film conditions were applied at the tool side and vacuum bag side of the laminates, to account for the heat transfer from autoclave temperature to part surface through convection. The effective film coefficients for both sides can be found in [2].This coupled temperature-displacement model took account of the residual stresses due to chemical and thermal shrinkage only.

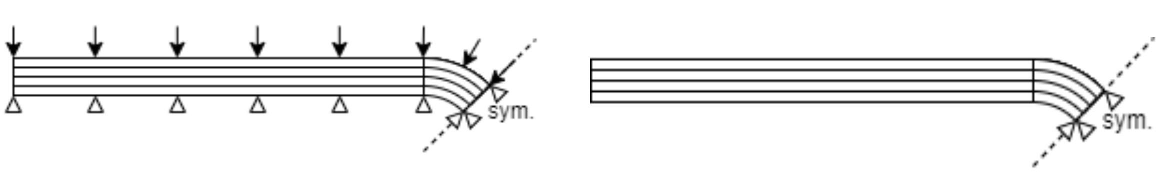

(a) Autoclave Cure (b) Tool Release

Figure 8 Geometry and boundary conditions for the two-step analysis of the L-shaped laminates

A follow-up static analysis was performed taking consideration of tool-part interaction only. The boundary condition for this case was depicted in Figure 9. Surface friction was applied as the equivalent residual stresses causing warpage in the flange part, the value of which were summarised in Table 2. Recall the total length in the curved direction for L-shaped specimen consists of two flanges and an arc, hence for specimens with a flange length of 60 mm, 90 mm and 120 mm, the corresponding friction of

35 kPa, 15.5 kPa and 7.9 kPa were employed. The induced spring-in angle was then super-positioned onto that obtained from the previous analysis.

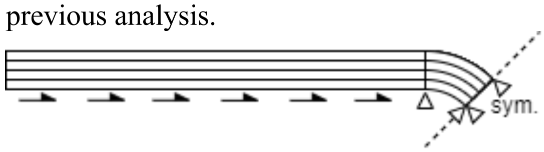

Figure 9 Boundary conditions for tool-part interaction analysis of the L-shaped laminates

4.3 Material properties

The nominal fibre volume fraction of the Hexcel IM7/8552 unidirectional prepreg used in this study was 57.7% and the nominal laminate density was 1570 kg/m^3. For the heat transfer analysis, the specific heat and thermal conductivity of IM7/8552 with temperature dependency are given in Table 3.

Temperature (°C)	Specific Heat (J/kgK)	Thermal Conductivity (W/mK)
25	857.41	0.84126
125	1130.99	1.02034
175	1289.75	1.12186

Table 3 Specific heat and thermal conductivity of IM7/8552 composites [3]

The cure kinetics model for resin 8552 has been thoroughly discussed in [4]. A summary for all the necessary parameters used in this analysis is listed in Table 4.

Constants	*[Unit]*	Value	Comments
H_T	*[J/kg]*	574,000	Total heat of reaction
E_a	*[J/mol]*	650,000	Activation energy
A	s^{-1}	70,000	Pre-exponential cure rate coefficient
m	-	0.5	First exponential constant
n	-	1.5	Second exponential constant
R	*[J/mol/K]*	8.314	Gas constant
C	-	30	Diffusion constant
α_{C0}	$[K^{-1}]$	-1.5148	Critical DoC at T=0 K
α_{CT}	-	5.171e-3	Constant accounting for temperature dependence

Table 4 Constants for 8552 cure kinetics model [4]

In the mechanical analysis, the expression of the CHILE constitutive model can be found in [2], the parameters used in which are listed in Table 5.

Parameters	Unit	Value	Comments
E_r^∞	*[MPa]*	4670	Unrelaxed resin modulus
E_r^0	*[MPa]*	4.67	Fully relaxed resin modulus
T_{C1a}	*[K]*	-45.7	Lower critical value for T* at 0 K
T_{C1b}	*[K]*	0.0	Variation of lower critical value for T* with increase in temperature
T_{C2}	*[K]*	-12	Upper critical value for T*
T_g^0	*[K]*	268	Glass transition temperature at DoC=0
α_{Tg}	*[K]*	220	Variation of glass transition temperature at DoC=0

Table 5 Parameters used for 8552 resin modulus development using CHILE model [2]

The effective mechanical properties of IM7/8552 unidirectional laminates were calculated using self-consistent micromechanical field model (SCFM). The properties derived using SCFM were compared against the FE-based model (FEBM) given by [5], shown in Table 6.

Properties	[Unit]	SCFM		FEBM[5]	datasheet
		Rubbery	Glassy	Glassy	Glassy
E_{11}	[MPa]	159,258	161,634	161,000	164,000
E_{22}=E_{33}	[MPa]	162.9	10,542	11,380	12,000
G_{12}=G_{13}	[MPa]	41.0	5,229	5,170	
G_{23}	[MPa]	40.8	3,542	3,980	
$\nu_{12} = \nu_{13}$	-	0.373	0.32	0.32	
ν_{23}	-	0.996	0.48	0.436	

Table 6 Effective mechanical properties of IM7/8552 unidirectional laminates using SCFM

The individual properties of fibre IM7 and resin 8552 are given in Table 7.

Properties	[Unit]	IM7[6]	8552[7]		Comments
			Uncured	Cured	
E_{11}	[MPa]	27,6000	4.67	4,670	Longitudinal Young's modulus
E_{22}=E_{33}	[MPa]	19,500	4.67	4,670	Transverse Young's modulus
G_{12}=G_{13}	[MPa]	27,000	11	1,704	In-plane shear modulus
G_{23}	[MPa]	7,800	11	1,704	Transverse shear modulus
$\nu_{12} = \nu_{13}$	-	0.28	0.5	0.37	In-plane Poisson's ratio
ν_{23}	-	-	0.5	0.37	Transverse Poisson's ratio

Table 7 Mechanical properties of IM7 fibre and 8552 resin [6, 7]

The coefficient of thermal expansion (CTE) and chemical shrinkage for IM7/8552 cross-ply laminates are given in Table 8.

Properties	[Unit]	Rubbery	Glassy	Comments
α_{11}^{t}	[$\mu\epsilon$/°C]	-	-0.1	Longitudinal CTE
α_{22}^{t}	[$\mu\epsilon$/°C]	-	31.0	Transverse CTE
α_{33}^{t}	[$\mu\epsilon$/°C]	-	31.0	Through-thickness CTE
α_{11}^{c}	[%]	0	-	Longitudinal CCS
α_{22}^{c}	[%]	0.48	-	Transverse CCS
α_{33}^{c}	[%]	0.48	-	Through-thickness CCS

Table 8 Thermal and chemical shrinkage for IM7/8552 cross-ply laminates [8]

5 RESULTS AND DISCUSSION

The spring-in angle comparisons between the numerical prediction and the experimental results are shown in Figure 10. The numerical prediction distinguishes chemical, thermal, and tool-part interaction contributions to the total spring-in angle. This investigation looked at geometric features of an L-shaped laminates, namely thickness, corner radius, and flange length effects. In general, the numerical prediction underestimates the spring-in angle, while the trends agree well with the experimental findings.

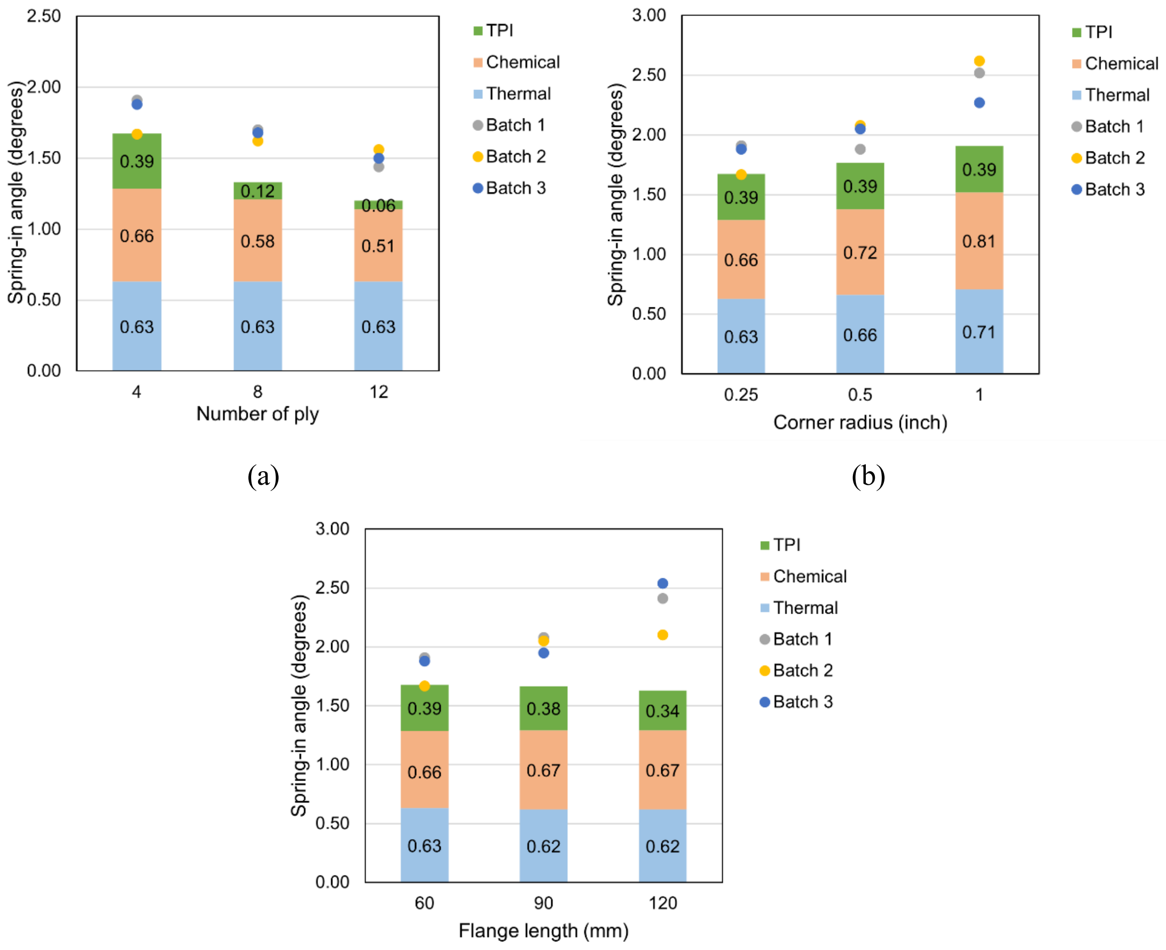

(c)

Figure 10 Comparison of experimental results and numerical predictions with varying (a) thickness (b) corner radius and (c) flange length of the L-shaped specimens

Figure 10 (a) reveals a clear trend in decreased spring-in angle with increasing laminate thickness. It was found that the thermal component does not vary much with changing thickness, while the contributions from chemical shrinkage and tool-part interaction decreased with increasing thickness. As bending stiffness increases, the warpage in the flange part decreases significantly. Figure 10 (b) indicates that increasing corner radius increases the spring-in angle contributions from chemical and thermal shrinkage. For the specimens with 1 inch radius, the average experimental finding shows 0.5° higher than the predicted value, this may have to do with underestimated value in tool-part interaction. In the static analysis, the friction was omitted in the curved part, the flange length was kept constant, therefore, the tool-part interaction was found to have equal effect on the final spring-in. In terms of curved part, plotting the arc-to-thickness ratio against the experimental spring-in angle gives a relatively linear relationship, as shown in Figure 11.

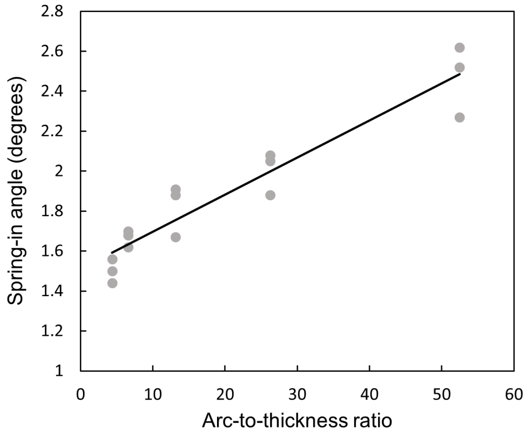

Figure 11 Arc-to-thickness ratio versus spring-in angle

It could be observed from the experimental results that the warpage in the flange part was more prominent in the specimen with longer flange length, which resulted in larger spring-in angle, shown in Figure 10 (c). However, such phenomena were not captured in numerical prediction. The chemical and thermal contribution to spring-in angle does not vary with changing flange length, while the effect from tool-part interaction was not clear. In the numerical simulation, the friction was calibrated from flat specimens, the value of which varies from 7.9 kPa to 35 kPa. Such value was calibrated from the average warpage measurement for two repeated specimens, based on the observed variabilities. Figure 12 shows the spring-in angle subjected to 50% variation in friction for the numbered specimen configurations in Table 1. For the case of 4-ply laminates, the spring-in angle varies from 0.2° to 0.6°.

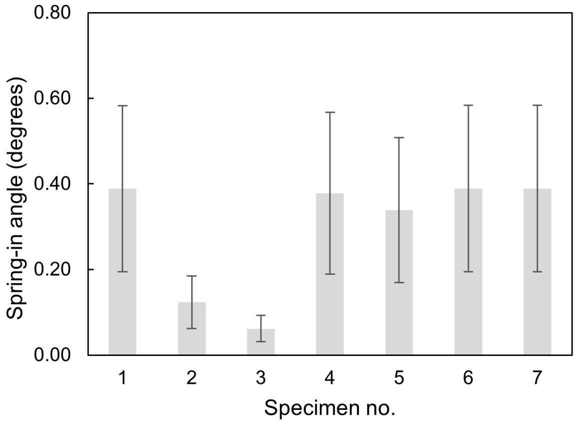

Figure 12 Spring-in angle due to tool-part interaction only

In terms of experimental uncertainties, one potential source of error could be the fibre misalignment during hand lay-up. Without a laser projection, the fabricated prepregs could be unbalanced if one of the plies was significantly misaligned. In this work, those specimens with unsymmetrical distortions were eliminated from the analysis since their induced spring-in angles were not reliable. A corner thinning effect was also observed from the specimens. The study found that the average cured single ply thickness at the flange part is 0.19 mm, while the average cured single ply thickness at the corner region is between 0.17 mm to 0.18 mm.

6 CONCLUSIONS

Although this study provides some insights into the geometric parameters affecting spring-in and warpage of L-shaped laminates, uncertainties cannot be ignored in the experimental and numerical procedures. Compared with direct modelling of the tool, the proposed semi-empirical method gives simpler, while reliable estimation of warpage. The main purpose of the current work is to show that corner component of spring-in was primarily the results of chemical and thermal shrinkage, while the warpage in the flange part was found to have great dependence on tool-part interactions.

ACKNOWLEDGEMENTS

This work was supported by the Engineering and Physical Sciences Research Council, UK [grant number EP/P006701/1]; through the EPSRC Future Composites Manufacturing Research Hub.

REFERENCES

[1] Albert C, Fernlund G. Spring-in and warpage of angled composite laminates. Composites Science and Technology. 2002;62:1895-912.
[2] Johnston AA. An integrated model of the development of process-induced deformation in autoclave processing of composite structures: University of British Columbia, 1997.
[3] Saad MT, Miller SG, Marunda T. Thermal characterization of IM7/8552-1 carbon-epoxy composites. ASME International mechanical engineering congress and exposition: American Society of Mechanical Engineers; 2014. p. V08BT10A091.
[4] Ersoy N, Potter K, Wisnom MR, Clegg MJ. Development of spring-in angle during cure of a thermosetting composite. Composites Part A: Applied Science and Manufacturing. 2005;36:1700-6.
[5] Obrien T, Krueger R. Analysis of Ninety Degree Flexure Tests for Characterization of Composite Transverse Tensile Strength. 2001.
[6] Kaddour A, Hinton M. Input data for test cases used in benchmarking triaxial failure theories of composites. Journal of Composite Materials. 2012;46:2295-312.
[7] Ersoy N, Garstka T, Potter K, Wisnom MR, Porter D, Clegg M, et al. Development of the properties of a carbon fibre reinforced thermosetting composite through cure. Composites Part A: Applied Science and Manufacturing. 2010;41:401-9.
[8] Ratcliffe JG, Czabaj MW, O'Brien TK. A test for characterizing delamination migration in carbon/epoxy tape laminates. 2013.